

Deep Domain Adaptation for Predicting Intra-Abdominal Pressure with Multichannel Attention Fusion Radar Chip

Hao Tang, Yanbo Dai, Dongchu Zhao, Zhiwei Sun, Fuqiang Chen, Yiliang Zhu, Huaping Liang, Hailin Cao,* and Lianyang Zhang*

Intra-abdominal hypertension (IAH) has gained increasing attention worldwide because of its prevalence and high mortality rate among intensive care unit (ICU) patients. Most current approaches of measuring intra-abdominal pressure (IAP) involve the use of sensors inside or attached to the body, which may, however, make daily monitoring inconvenient. This paper proposes a noninvasive and contactless system to learn the relationship between the passive mechanical behavior of the abdominal wall with millimeter-wave (mm-wave) frequency-modulated continuous wave (FMCW) radar and an IAP sensor via a deep learning approach. We correlated the IAP variance with the mobility measures of the abdominal wall and proposed Pearson-coefficient-guided domain adversarial neural network (PCG-DANN) to learn the mapping relationship. To validate the efficacy of our proposed method, a stable intra-abdominal hypertension/abdominal compartment syndrome (IAH/ACS) model using swine was established to evaluate the mobility of the abdominal wall under different intra-abdominal pressures with multichannel mm-wave FMCW radar. The superiority of the proposed method is demonstrated by comparing with other neural network structures and mostly adopted sensor-based methods. These preliminary results confirm that the new methodology for evaluating IAP nonlinearity is promising and that it can serve as an important diagnostic and treatment reference for patients with IAH.

1. Introduction

Intra-abdominal hypertension (IAH), also referred to as increased intra-abdominal pressure (IAP), may lead to abdominal compartment syndrome (ACS).^[1] IAH has direct effects on the functions of abdominal organs, such as the kidney and liver, and organs outside the abdominal cavity, including the brain, cardiovascular system, and lungs. As a result, IAH has gained attention from an increasing number of physicians in intensive care units (ICUs).


Therefore, measuring and monitoring the IAP is essential for daily management and diagnosis. Direct laparoscopic measurement with an intra-abdominal catheter is the most accurate method; however, it is expensive and requires highly trained personnel.^[2] The indirect urethral measurement, which is often referred to as trans-bladder measurement,^[1] is the most widely used and reliable method of monitoring IAP; however, this approach can result in urinary tract infections or urethral injury.^[3] Special sensors or probes inserted

into the rectum or intravaginally have also been used for IAP measurements; such probes convert mechanical effects into electrical signals.^[4] Gastric or nasogastric tubes inserted into the stomach also provide accurate IAP results.^[5] However, these methods remain in vivo or invasive, are still relatively inconvenient to install, and may induce patient discomfort.

In clinical practice, the palpation of the abdominal wall tension (AWT) is used to evaluate the ability of an individual to regulate IAP. Different types of sensors have been developed to measure AWT related to IAP changes.^[6–8] Specifically, one study found that the tension increases in the abdominal wall are directly correlated to the rise of the IAP by comparing a simultaneous recording of the IAP measured as anorectal pressure and the AWT measured with four sensors attached to a trunk brace.^[6] Nevertheless, the IAP can also be considered as a distributed load applied to the internal abdominal surface. The in vivo passive mechanical behavior of the abdominal wall mostly depends on the IAP. Multiple cameras were used to optically track a patient's skin surface and compare it to the ideal position with submillimeter accuracy.^[9] The pressure–displacement curves confirmed that the mobility of the abdominal wall is nonlinear and related to the IAP load.

H. Tang, D. Zhao, H. Liang, L. Zhang
Wound Trauma Medical Center
State Key Laboratory of Trauma, Burns and Combined Injury, Daping
Hospital
Army Medical University
Chongqing 400042, China
E-mail: dpzhangly@163.com

Y. Dai, Z. Sun, F. Chen, Y. Zhu, H. Cao
Chongqing Key Laboratory of Space Information Network and Intelligent
Information Fusion
Chongqing University
Chongqing 400044, China
E-mail: hailincao@cqu.edu.cn

 The ORCID identification number(s) for the author(s) of this article can be found under <https://doi.org/10.1002/aisy.202100209>.

© 2022 The Authors. Advanced Intelligent Systems published by Wiley-VCH GmbH. This is an open access article under the terms of the Creative Commons Attribution License, which permits use, distribution and reproduction in any medium, provided the original work is properly cited.

DOI: 10.1002/aisy.202100209

When the muscle is considerably deformed for each level of pressure at low pressures, the tissue becomes more rigid, and the strain increment for each mmHg of pressure becomes significantly lower at high pressures. However, optical approaches require the patient's surface to be exposed, and their performance is often affected by individual body shape differences. To date, there is no model that quantitatively describes the relationship between the AWT and IAP.

Millimeter waves (mm-waves) refer to electromagnetic waves in the frequency range of 30–300 GHz. Clothing and other organic materials are transparent to mm waves, which is how the technology employed in airport security is used to detect weapons and other dangerous objects. Mm-wave radar is also widely used in the field of gesture recognition and sleep monitoring owing to its excellent performance in detecting minimal vibrations.^[10–12] Radars in the millimeter waveband are also widely adopted in scenarios requiring the measurement of small displacements. For instance, various millimeter-wave radars, such as continuous wave (CW) radar, ultrawideband (UWB) radar, and frequency modulated continuous wave (FMCW) radar, are often applied to measure and monitor the vital biological signals of respiration and heart rates. Unlike the conventional vital signal detection method, which mainly acquires biological data through contacted wearable sensors or sticky electrodes, the radar system can obtain desirable data in a wireless fashion.^[13,14] The noncontact characteristic of the radar system does not induce discomfort to patients and can significantly simplify the complicated operating procedures of the conventional method based on contacted sensors or electrodes. Among all these radar systems, the FMCW radar system outperforms other radar systems in detecting small displacements and biological vital signals owing to its higher range and speed.^[15] Moreover, it can extract and distinguish the separated information of different individuals from multiple targets, enabling the single radar system to simultaneously measure the vital signals of multiple targets.^[16]

Artificial deep neural networks are now commonly used in medical signal processing and other relevant fields as an effective way to extract valuable features or patterns from medical images or sequential signals, such as electroencephalogram (EEG) signals. Moreover, owing to the limitations caused by the individual differences across several subjects, a domain adaptation (DA) is added to a deep neural network to distinguish the domain-invariant features from various subjects. For instance, different neural networks with DA have been proposed to recognize the emotions from extracted EEG signals and show their superiority over other methods.^[17–19]

This article presents a novel IAP measurement system based on multichannel mm-wave FMCW radar, and the system's noninvasive and contactless characteristics can make daily monitoring of IAP easier to implement. The proposed IAP measuring system can significantly simplify the operating procedures induced by trans-bladder measurement and pressure-sensor-based approaches, which are currently the most adopted approaches in the clinical environment. The discomfort caused by measuring IAP via these widely adopted methods can also be reduced. Taking advantage of the outstanding performance

of the mm-wave FMCW radar system in measuring small displacements, the proposed IAP measuring and monitoring system takes the tension-modulated displacement signal of the abdominal wall acquired from the mm-wave FMCW radar as the input and learns the relationship between the input mobility data and the measured IAP value using the deep learning approach. Furthermore, we propose a new deep learning network under the domain adversarial neural network (DANN) framework. In such cases, the individual differences in the experimental animals can be reduced, and invariant features are much more likely to be extracted to build a link between the radar signal and the IAP. A convolutional recurrent neural network (CRNN) was applied in the proposed deep learning framework to extract valuable features from the input data. A discrete wavelet transformation (DWT) layer is also added to the feature extractor to extract explicitly valuable stochastic features because the inherited local awareness structure constrains the ability of the RCNN to draw the overall features. To further improve the accuracy of the regression task, the Pearson-coefficient-guided (PCG) regressor is proposed for the first time to emphasize the mobility features between all the extracted features under the hypothesis that the features that are more reasonable and welcomed are more likely to have a direct relationship with the IAP value.

To verify the effectiveness of the proposed method, experiments were conducted on swine using the IAH/ACS model to collect sufficient data, which enabled us to establish a dataset for training the neural network. We demonstrate the superiority of the proposed method over sensor-based approaches by achieving a mean absolute error value of 0.64 on the test dataset, which contains brand new data collected from a pig that was not included in the training or validation set.

The contributions of this paper can be summarized as follows:

- 1) We propose a new, noninvasive, and contactless method for measuring IAP with multichannel mm-wave FMCW radar.
- 2) We present a Pearson-coefficient-guided domain adversarial neural network (PCG-DANN), which reduces the difference between various individuals; thus, the domain-invariant features are much more likely to be extracted to establish the relationship between the features and the IAP.
- 3) DWT is added to the feature extractor to explicitly draw the stochastic mobility features to augment the ability of the neural network in extracting features of the overall time series.

Compared with the most adopted pressure sensor-based methods, this novel method is *ex vivo*, noninvasive, and contactless. It can measure the IAP from a distance, which is convenient for continuous monitoring.

The rest of the article is organized as follows. Background information of the proposed method, including physiological support, system overview, preprocessing procedures, and DWT technique, is reviewed in Section 2. Section 3 elaborates on the experimental setup. The subsequent section focuses on the proposed deep learning neural network: the PCG-DANN. Section 5 focuses on a specific data analysis and a discussion where the effectiveness of the proposed method is verified. Finally, the conclusions of this study are drawn in Section 6.

2. Background

2.1. Physiological Support and System Overview

A recent numerical model of abdominal wall mechanics notes the link between the displacement of the abdominal wall and the IAP.^[20] The shift due to muscle contraction and relaxation is also affected by different IAP values. Thus, the mm-wave FMCW radar, which can detect minimal displacement, has been proposed to measure the shift of the abdominal wall. The corresponding IAP was measured using the trans-bladder measurement method. The model takes the radar signal as the input and generates the corresponding IAP value, which can be obtained by training a deep learning network. **Figure 1** shows an illustration of the proposed method.

2.2. FMCW Radar Signal Preprocessing

The mm-wave sensor used in this study was an IWR6843 from Texas Instruments. It operates at 60–64 GHz with one of three transmit antennas (TX) enabled, and all four receive antennas (RX) enabled data collection.^[16] The radar signal bouncing back from the abdominal wall is collected by the four receiver pairs and is presented in the I/Q form.

To obtain the desirable abdominal displacement signal, specific signal preprocessing procedures, which are presented in **Figure 2**, are proposed in this article. After acquiring the intermediate frequency (IF) signal, range-FFT is performed for each of the transmit–receive antenna pairs, and the obtained data are rearranged into the format of the RF image illustrated in **Figure 2**. The mean value along each slow-time axis was subtracted to avoid the distraction from the static components. In such cases, objects that occupy different range bins can be distinguished and separated from one another. The abdominal displacement signal can also be extracted under the hypothesis that there is only one nonstatic object in the field of radar. Thus, the range bin with the highest energy can be extracted as the desirable signal that bounces back from the abdominal wall. The phase value of the extracted signal is then computed using the arc tangent operator and unwrapped to obtain the actual phase information, as expressed in Equation (1). Subsequently, the difference between successive phase values was computed to prevent any phase drifts.

$$\varphi = \text{unwrap}[\arctan\left(\frac{Q}{I}\right)] \quad (1)$$

The extracted differential phase value, which is related to the minimal displacement through the equation $\Delta\varphi = \frac{4\pi}{\lambda} \Delta R$,^[16] can be used to present the minimal vibration of the abdominal wall. In the aforementioned equation, λ represents the wavelength of the emitted wave, and ΔR represents the minor shift. The extracted abdominal displacement signal, whose representation in the time domain is illustrated in **Figure 2**, should be denoised because undesirable signals or noise may be considered. In this case, a digital low-pass Butterworth filter with a cutoff frequency of 2 Hz was implemented to denoise the obtained signal and improve the signal-to-noise ratio. Following the preprocessing procedures, the denoised abdominal displacement signal can be extracted from the original radar signal.

2.3. Discrete Wavelets Transform

The DWT is a commonly used digital signal preprocessing technique that can help to better extract the time–frequency features of the time series. It decomposes the input signal data from the time domain into a series of components at different frequency intervals. By applying this technique to the proposed method, the prediction accuracy can be significantly enhanced.

The method proposed in 1989 and developed by Mallet is widely accepted as the gold standard for calculating the DWT. An arbitrary signal $s(t)$ can be decomposed into its multiresolution form as follows

$$s(t) = \sum_k a_{M,k} \frac{1}{\sqrt{2^M}} \varphi\left(\frac{t}{2^M} - k\right) + \sum_j \sum_k d_{j,k} \frac{1}{\sqrt{2^j}} \psi\left(\frac{t}{2^j} - k\right) \quad (2)$$

where $a_{M,k}$ and $\varphi(t)$ denote the approximation coefficients at level M and the companion scaling function, respectively.^[21] Equation (2) can be transformed into another form using $A_M(t)$ and $D_j(t)$ to replace $a_{M,k} \frac{1}{\sqrt{2^M}} \varphi\left(\frac{t}{2^M} - k\right)$ and $\sum_k d_{j,k} \frac{1}{\sqrt{2^j}} \psi\left(\frac{t}{2^j} - k\right)$, respectively. The detailed signal $D_j(t)$ can then be extracted using Equation (3)

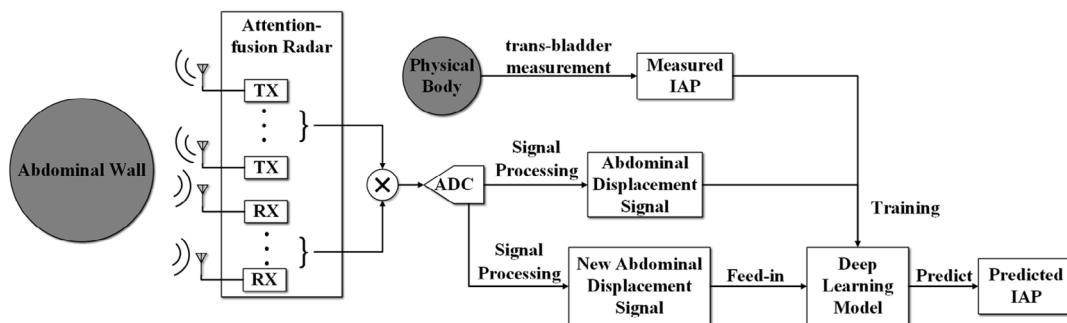


Figure 1. Illustration of the proposed method.

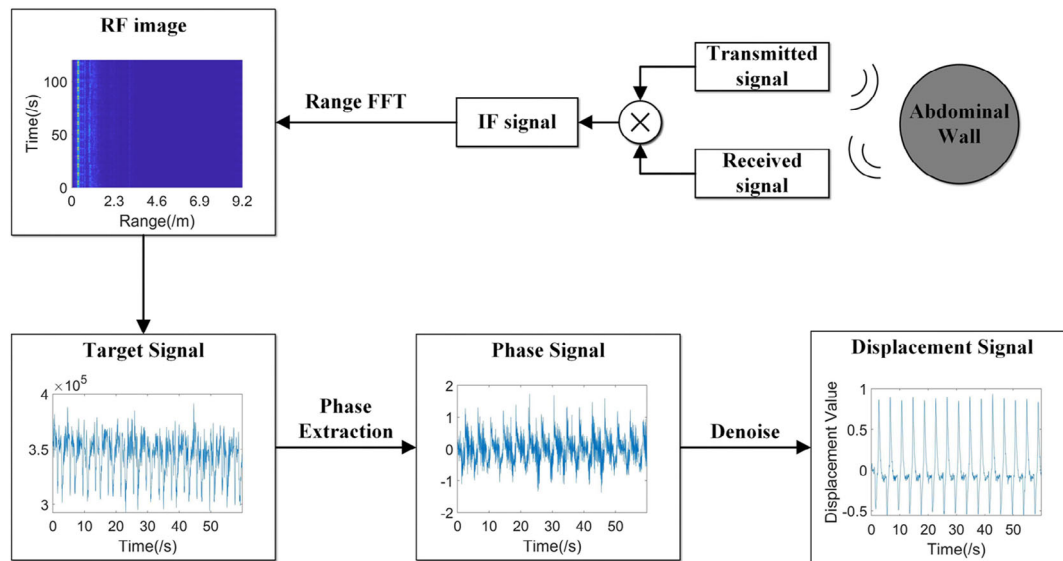


Figure 2. mm-wave radar signal preprocessing flow. The RF image and the displacement signal of the data collected in the experiment are presented in the figure.

$$s(t) = A_M(t) + \sum_j D_j(t) \quad (3)$$

The quality of the detailed signal can be affected by different wavelets that have different time–frequency domain characteristics. Wavelets were selected based on sampled data. It is better to choose the db and sym wavelet families when there are enough samples in the input data because of their robustness regardless of the input data properties. The longer filter lengths of other wavelet families may undermine the quality of the extracted signal compared to the db and sym wavelet families.^[22] Another parameter that influences the quality of the decomposed component is the decomposition level. A greater decomposition level, which can provide more detailed information on the input signal, proportionally leads to a higher computational cost. The maximum of the wavelet decomposition level is constrained jointly by the length of the sampled signal and the type of mother wavelet.^[22]

In this work, the db8 and sym8 wavelets are used as mother wavelets in the Mallet decomposition algorithm, and the maximum decomposition level M was set to 3. After decomposing the signal into a set of components from different frequency intervals, six handcrafted stochastic features, as listed in Table 1, were computed for each of the decomposed components.

3. Experimental Section

3.1. Animal Model of Peritonitis

Animal experiments complied with international and national animal testing regulations. The experimental protocol was approved by the Laboratory Animal Welfare and Ethics Committee of the Third Military Medical of the Chinese People's Liberation Army University (AMUWEC20201513). Five landrace pigs (two males and three females) aged

Table 1. Description of the extracted features, where s denotes the sequence of the detail signal.

Feature	Description
Maximum Value	$\max(s)$
Minimum Value	$\min(s)$
Mean Value	$\mu = E(s)$
Standard Deviation	$\sigma = E[(s - \mu)^2]^{1/2}$
Skewness	$E[(s - \mu)/\sigma]^3$
Energy	$\sum s^2$

approximately three months and weighing 28–32 kg were used for the experiment. All the animals received the same anesthesia and mechanical ventilation regimen during the study. Trans-bladder measurements were performed to measure IAP. An abdominal puncture was performed at the navel, and an 8-FR abdominal drainage tube (Guangdong Baihe Medical Technology Co., Ltd.) was placed.

3.2. Measuring IAP via Trans-Bladder Measurement and mm-Wave FMCW Radar

The IAP was measured using trans-bladder measurements developed in the 2013 Guidelines of the World Society of the Abdominal Compartment Syndrome (WSACS). Malbrain's modified sterile IAP measuring device was attached to the catheter.^[1] The experimental pigs were placed in a supine position. After emptying the bladder, 25 ml of normal saline was injected into the bladder through a suprapubic cystostomy fistula. The zero-scale line of the equipment was measured with the level of the pubic symphysis of the pig's body. The end-expiratory reading of the water column height was taken as the measurement result.

The average value of the measurement results was taken as the final result and converted into mmHg. Meanwhile, the mm-wave FMCW radar was placed toward the abdominal wall of the animal from approximately 1 m away to obtain the displacement signal of the abdominal wall of the animal. The ventilator shown in **Figure 3** was used to maintain the breathing of the animals.

4. PCG-DANN

4.1. DA

DA aims to enable the deep learning model to predict the labels from multiple domains discriminatively given the data from the test dataset in the presence of drift between the training and test distributions. For the specific scenario, the model trained on one cohort may fail to predict the outcome given the data of another cohort due to differences in age, physical state, or health condition. In such cases, a model that can extract invariant features and build a link between these domain-invariant features and outcome labels is more welcomed and is much more likely to be applied in clinical environments. Previous studies on DA have focused on fixed feature representations, including linear and nonlinear features.^[23–26] While recent studies have embedded DA into the process of training neural networks using adversarial learning,^[27] Based on the proposed theory,^[28] the desirable representation for a cross-domain transfer cannot distinguish the domain from the input observation. The domain adversarial neural network inserts a domain classifier in the network to reduce the ability of the network to discriminate the domain of the input data. Thus, the input data must combine both the training and testing sets to train the domain classifier, whose task is to determine whether a piece of data comes from the training set or testing set. Only the abdominal

displacement signals in the testing set were included in the input data in the training stage, and the labels were not included. The domain classifier, shown in **Figure 4**, is connected to the feature extractor via a gradient reversal layer (GRL), which multiplies the gradient with a certain negative constant within the back-propagation-based training method. The GRL works as an identical transformation in forward propagation while changing the sign of the gradient from the subsequent layer before passing it to the preceding layer. No additional parameters are required in the GRL, and it is convenient to implement using existing deep learning programming libraries. In such cases, the accuracy of the domain discriminator decreases during the training stage; thus, the domain-invariant features are much more likely to be learned by the neural network.

To eliminate individual differences and learn domain-invariant features, we adapted and adjusted the DANN as the framework of the proposed deep learning method. The DANN framework comprises three components: a domain discriminator, which is described earlier, a feature extractor used to draw features set manually or learned automatically by the neural network, and a PCG augmentation regressor, which aims to bridge the extracted features with the label values. The following section illustrates the rest of the proposed neural network structure, which is shown in Figure 3.

4.2. Feature Extractor

4.2.1. Learning Features via CRNN

Convolutional neural networks (CNNs) have achieved significant success in the fields of computer vision and pattern recognition. Hierarchical features can be learned through the training stage of

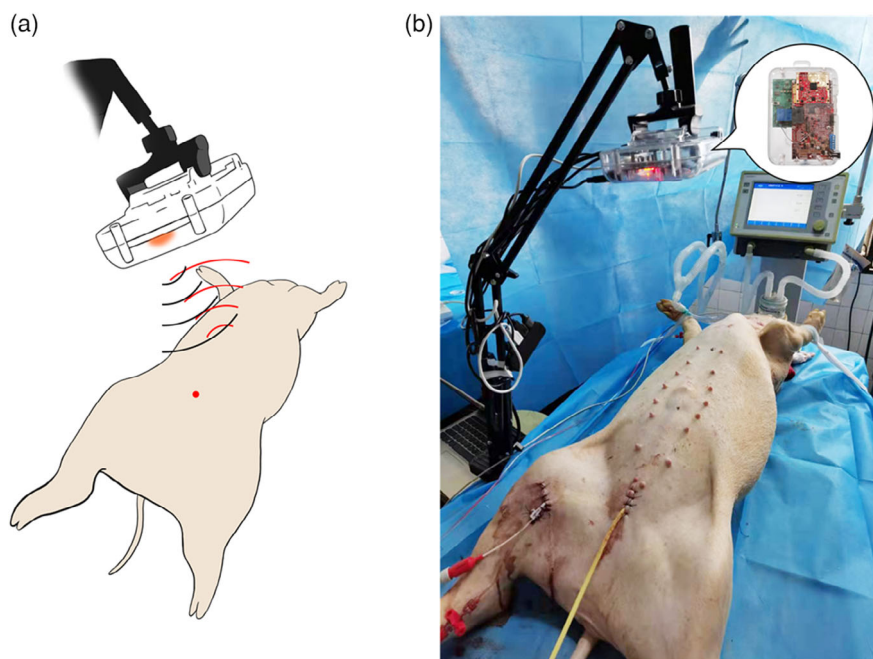


Figure 3. Animal experiment setup. The mm-wave FMCW radar shown specifically in (b) is used to measure the abdominal displacement of the animal. The trans-bladder measurement is performed to measure IAP and the ventilator shown in (b) is used to maintain the breathing of the animal.

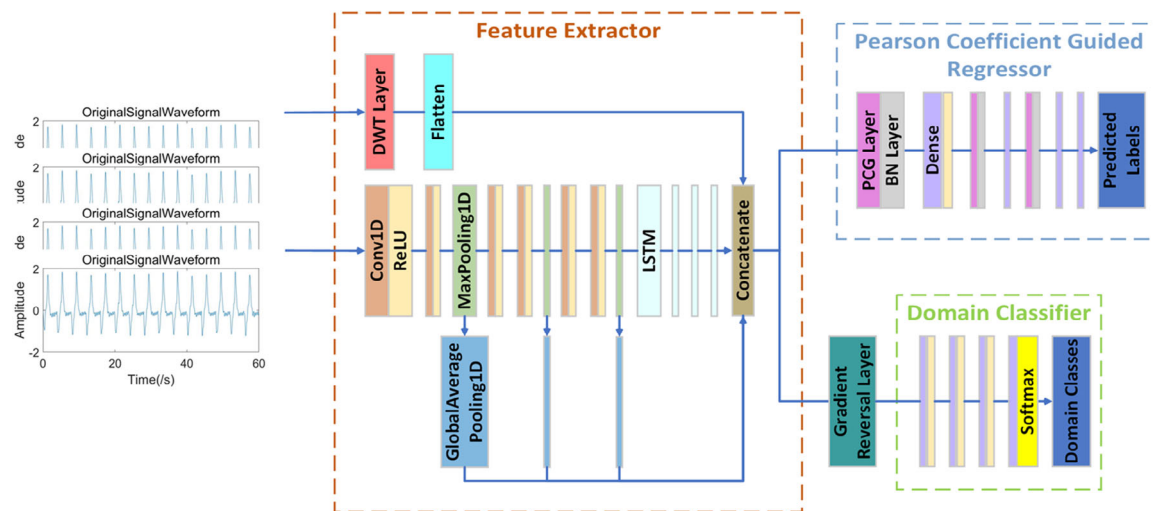


Figure 4. Illustration of the proposed PCG-DANN.

a neural network. Higher-level features can be constructed by extracting preceding features. Moreover, as the training procedure continues, CNNs can achieve better performance than features that are set manually by experience through a large amount of training.^[29] Recurrent neural networks (RNNs) have also been very successful in the field of various sequence prediction or sequence labeling tasks. RNNs can learn features that represent the sequence relationships. Several variants, including long short-term memory (LSTM) and gate recurrent units (GRUs), have been proposed to solve the vanishing gradient problems that traditional RNNs may encounter during the training stage.^[30]

In this article, a CRNN, which combines the properties of CNN and RNN, is proposed to extract features from the denoised abdominal displacement signal. The input data first go through three neural network blocks comprising two 1D CNN layers and a max-pooling layer. Features can be extracted primitively through these blocks, and the number of sequence units can also be reduced to shorten the computational time required by the following RNN layers. It is commonly thought that relying solely on the last CNN layer in a hierarchical forward-propagation neural network may not extract sufficient valuable information from the training data.^[31] The low-level information may also be abandoned during the forward propagation procedure. Thus, a global average pooling layer is applied after every CNN block to preserve the low-level features. The features extracted via each CNN block through forward propagation can be gathered as a part of the final extracted features. After three CNN blocks, four LSTM layers with dropout coefficients were applied to draw sequential information. The features extracted by the LSTM block and the features extracted by the CNN blocks are combined as the features extracted by the CRNN. Figure 3 shows the structure.

4.2.2. Extracting Global Mobility Features Through the DWT Layer

While the CNN seems to dominate the field of computer vision and pattern recognition, whose input data are mostly in the

format of two dimensions, its applications in sequential data are not very popular. This may be the reason that the inherited structure of the local-aware perceptron is inapplicable for extracting valuable features from sequential data. The overall information may be corrupted through a convolutional operation. The DWT described previously is a commonly used digital signal preprocessing technique that can help better extract the time-frequency features of the time series. Owing to this ability, it has been widely used in image denoising and edge-feature enhancement scenarios.^[32,33] In such cases, the DWT technique is used in this work to draw handcrafted stochastic features from different intervals of the original abdominal displacement signal and to compensate for the loss of panoramic information if there are only features extracted by the CRNN.

4.3. PCG Regressor

The regressor designed in the neural network aims to bridge the extracted features with IAP labels. A commonly used regressor in most sequential regression tasks is a multilayer perceptron (MLP) with the number of hidden units in the last layer set to one and without an activation function. In this article, we propose a novel regressor, which is shown in Figure 5, based on a PCG layer for the first time to emphasize the extracted features that are linearly correlated with the labels. We propose an intuitive hypothesis that a feature that is more linearly correlated with the IAP value is more acceptable. Let $X \in \mathbb{R}^{d \times f}$ be the extracted features, and d, f be the number of input data in the minibatch and the number of features, respectively. Let $Y \in \mathbb{R}^d$ be the index of the data in the minibatch. In such cases, we sort the data in the input minibatch in ascending or descending order. The linear correlation between the features and the IAP labels can then be calculated by computing the Pearson correlation coefficient, which is expressed in Equation (4), between the features and the index of the minibatch data. A sigmoid activation function is then applied to the calculated coefficients

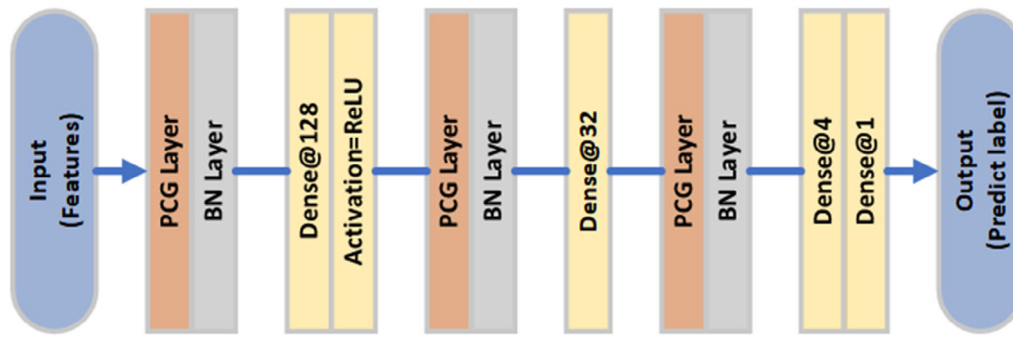


Figure 5. PCG Regressor.

$$\rho(X, Y) = \text{sigmoid}\left(\frac{E[(X - \mu_X)(Y - \mu_Y)]}{\sigma_X \sigma_Y}\right) \quad (4)$$

The coefficients $\rho \in \mathbb{R}^f$ are multiplied with the extracted features to emphasize the features that have a strong linear correlation with the labels. These operations can be wrapped in the PCG layer and can be easily implemented using existing deep learning programming libraries, such as TensorFlow and PyTorch. The PCG layer does not require additional parameters; thus, the computation time consumed will not increase if the PCG layers are added to the network. A batch normalization (BN) layer was added after each PCG layer to make the network converge more easily.

5. Results and Discussion

5.1. Implementing Details

The data for the five pigs were collected once the peritonitis model was established in the animal experiment. Each piece of the data, which lasted 60 s and contained four channels, was collected every half an hour since the beginning of the experiment. To simulate the clinical environment and to avoid the leakage of the frequency spectrum, a hamming window that lasted 25 s and shifted every 5 s was applied to segment the entire time series into eight smaller pieces. The sampling rate of the radar was set to 20 Hz. In these cases, each small piece of the time series contained 500 points and four channels. Data collected from one of the five pigs were used as the testing dataset to verify the ability of the model to learn domain-invariant features. The training and validation sets consisted of data collected from the remaining four pigs, and the separation ratio was set to 9:1.

5.2. Network Performance

We demonstrate the performance of the PCG-DANN in predicting the IAP value, given the corresponding abdominal displacement signal through a comparison with other neural network structures, which is currently the most adopted method to measure IAP in clinical environments. The performance of a recent sensor-based approach that adopted a novel sensor by inserting a disposable transducer inside the patient's body was also evaluated to demonstrate the superiority of the proposed method.^[34]

The performance of various neural networks was also evaluated to demonstrate the effectiveness of the proposed PCG and DWT techniques. In this work, a normal CRNN with a MLP as the regressor is treated as the baseline of the proposed sequential problems. Neural networks and their variants are widely used in the fields of grid fault detection and fault diagnosis,^[22,35] whose input signals are also one-dimensional. The short-time Fourier transformation (STFT)-based method, which transfers the time series into a time–frequency map and feeds into the 2D-CNN, is another baseline to be compared. STFT is a widely adopted method for processing sequential signals in the time domain by transforming time series into 2D time–frequency diagrams. Valuable features in the frequency–time map extracted from music signals can be drawn using a pretrained VGG neural network.^[31] In such cases, a VGG-like neural network can also be adopted to build the mapping between the acquired radar signal and the IAP. To verify the effectiveness of the proposed PCG layer, a comparison between the proposed PCG-DANN with the PCG layer and the vanilla DANN with the CRNN and DWT layers as its feature extractor and without the PCG layer in the regressor was conducted. We also compare the proposed PCG-DANN with the SE-DANN, which has the CRNN and DWT layers as its feature extractor and has a regressor with a squeeze-and-excitation (SE) block. The SE block explores the relationship between different channels and produces channel-wise weights to enhance the channels,^[36] which are thought to be more informative through the training process and suppress the less important ones. The comparison can also help verify the correctness of the proposed intuitive hypothesis in Section 3.3. The performance of a variant of the proposed PCG-DANN that does not adopt the DWT technique in the feature extractor to compensate for the panoramic information was also evaluated to verify the effectiveness of the DWT technique. **Figure 6** shows an illustration of the comparison of the testing dataset. **Table 2** presents the results for the training and validation sets.

As shown in Figure 6 and Table 2, the performance of the proposed PCG-DANN surpasses that of the baselines and other neural network structures. Its mean absolute error on the testing dataset is the lowest among all the other neural network structures, and the trend of the predicted mean value is roughly the same as the label values. The poor performance of the STFT-based method, which achieves the lowest regression accuracy among all the listed neural network structures, indicates that the 2D-CNN method, which prevails in computer vision, is

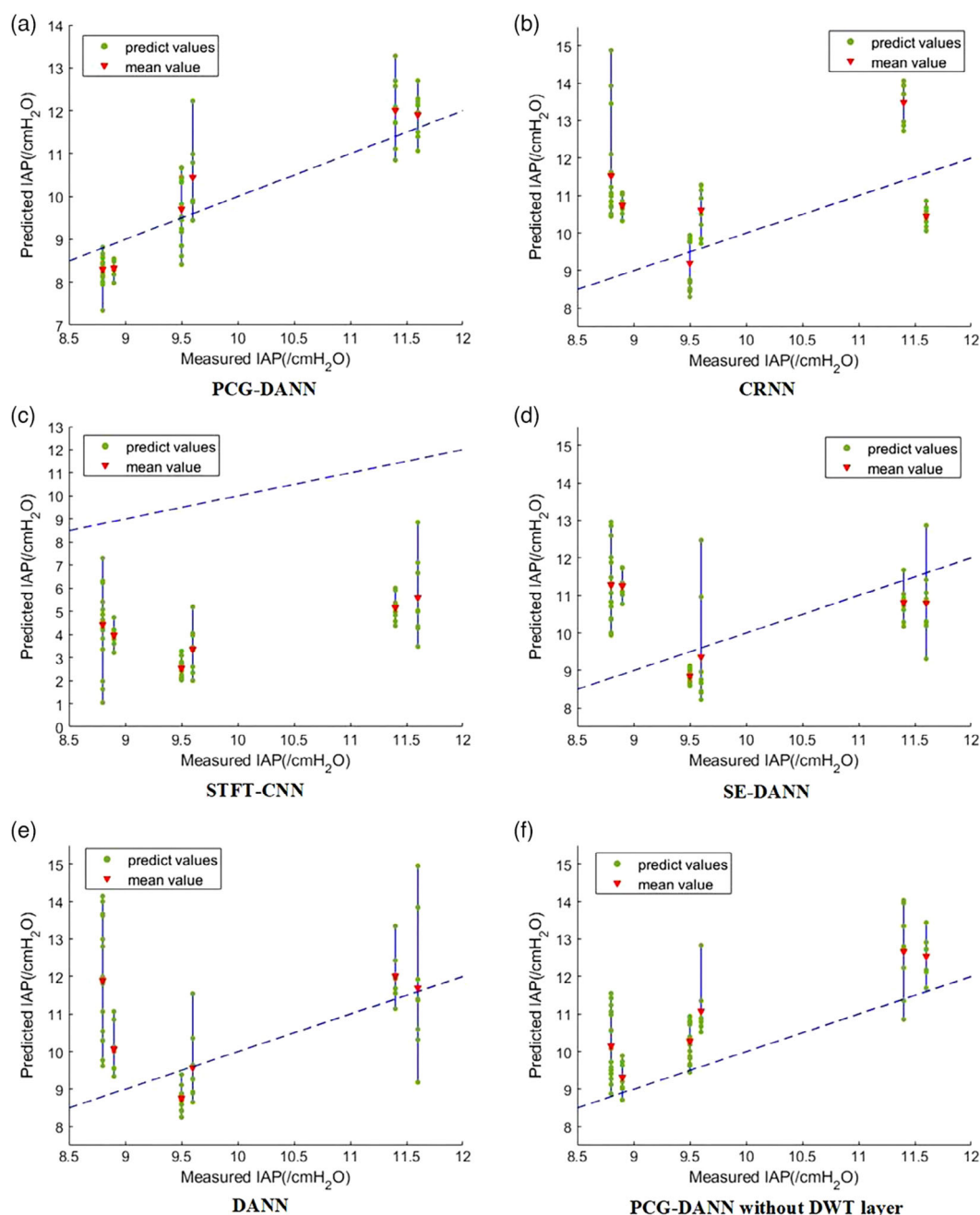


Figure 6. Different network performance on the testing dataset. a) PCG-DANN, b) CRNN, c) STFT-CNN, d) DANN with SE blocks (SE-DANN), e) DANN, f) PCG-DANN without DWT layer.

inefficient in the field of time-series signals in given scenarios. This is mainly because features that represent intra-sequential relationships are more informative and valuable given sequential data. Typical VGG-like neural network structures cannot model intra-sequential relationships and fail the regression task.

The effectiveness of the proposed PCG layer can be verified by comparing the neural network structure with the PCG regressor and the structure with the SE regressor. The higher performance

of PCG-DANN on every evaluating dataset also demonstrates the effectiveness of the proposed hypothesis in Section 3.3, which has a strong linear correlation with the output labels in the regression task of biological signals. The superiority of the PCG technique can also be demonstrated by comparing the performance of the PCG-DANN and the DANN, which does not have a PCG regressor. The PCG-DANN evaluated on each of the datasets outperforms the original DANN, showing the advantage of the proposed hypothesis and the PCG technique.

Table 2. Various neural network structure performances are presented in terms of the mean absolute error on different datasets. The performance of the sensor-based approach is also listed to serve as a contrast.

Networks	Datasets	MAE	Networks	Datasets	MAE
PCG-DANN	Training	0.78	DANN	Training	1.32
	Validation	0.74		Validation	1.42
	Testing	0.64		Testing	1.45
CRNN	Training	0.28	PCG-DANN without DWT	Training	0.84
	Validation	2.53		Validation	0.88
	Testing	1.6		Testing	1.07
STFT-CNN	Training	2.2	Sensor-based Approach		1.39
	Validation	2.54			
	Testing	5.75			
SE-DANN	Training	1.02			
	Validation	1.15			
	Testing	1.46			

The better performance of the neural network structure with the DWT layers compared with the structure without DWT layers verifies the significance of the DWT technique and illustrates that the extracted panoramic features are essential for bridging the input signal and the output label. It may also show that the DWT layer can compensate for the loss of the panoramic information caused by the built-in local-aware perceptron structure inside the CNN.

The effectiveness of the proposed method can also be seen through a comparison between the sensor-based approach, which achieves a mean absolute error value of 1.39, and the absolute error ranges from 0.3 to 4.1 based on the data collected from 25 patients.^[34] However, the data collected in this study were from animals rather than patients in clinical environments, and the differences between animals and patients were not considered. Further research on patients in clinical settings is required.

5.3. Influence of Model Parameters

The influence of the different settings of the parameters in the neural network is discussed in this section. For the proposed PCG-DANN, the accuracy of the PCG regressor and the generalizability of the entire network is significantly influenced by the output weight ratio between the domain discriminator and the regressor. In such cases, experiments were conducted by applying the proposed neural network with different settings in the output weight ratio on the same dataset to analyze their effect on the PCG-DANN.

As shown in **Figure 7**, the performance of the neural network with an output ratio of 1:4 surpassed that of the network with the other output weight ratios. Generally, a low ratio between the output weight of the regressor and the domain discriminator leads to a better performance for the entire network. The high ratio between the domain discriminator and the regressor elevates the ability to extract more domain-invariant features while simultaneously increasing the difference between the predicted values

and the labels. Thus, the DA mechanism can be seen as a trade-off between accuracy and generalizability.

5.4. Discussion

The proposed method, which can measure IAP wirelessly, is superior to the mostly adopted sensor-based methods. The Pearson coefficient between the labels and the predicted values was 0.89, indicating a strong correlation and demonstrating the correctness of the proposed methods. In such cases, this novel noninvasive and contactless technique exhibits broad application prospects in the daily care of future ICUs. It can significantly simplify the measuring and monitoring procedures and will not induce any discomfort when applied to patients, making the daily monitoring of IAP much easier to implement. The proposed IAP measuring system can also be extended to monitor multiple targets within one hospital ward because the mm-wave FMCW radar can acquire biological vital signals of multiple targets; this aspect will be studied in the future. These properties make the proposed method a promising technique with broad application prospects in the daily nursing of future ICUs.

This experimental study is not exempt from some limitations. First, the number of specimens used for data collection should be increased to learn the nonlinear relationship between the mobility of the abdominal wall and the IAP. In addition, this measurement method should be applied to human tissue and experimental data should be collected to verify the effectiveness of the proposed method when applied to solve real-world problems because the main objective of this methodology is to be applied to ACS diseases in humans. Furthermore, the robustness of the proposed IAP measuring system needs to be investigated further for the system to be applied in real-world scenarios. The quantitative relationship between the mechanical configuration, such as the displacement height and angle between the mm-wave FMCW radar, and patient requirements, to be further defined. The robustness of the system against common interference, such as mechanical perturbations and electromagnetic interference, should also be explored. It is rather important for the performance of the system, which is meant to be used for clinical purposes, to remain stable when the system is disturbed either by improper mechanical operation or by electromagnetic interference induced by other electronic devices. Additional work is required to enable the measurement system to be applied in a real clinical environment. These limitations will be explored in future research because of the limited size of the data collected from the animal experiments described in this work.

Despite these limitations, this work presents a new methodology for evaluating IAP nonlinearity, which can serve as an important diagnostic and treatment reference for patients with IAH. It is a promising technique to be applied in real-world clinical environments.

6. Conclusions

IAH has gained increasing attention in ICUs worldwide. However, the approaches used to measure and monitor IAP remain invasive or require contact with patient bodies; this makes

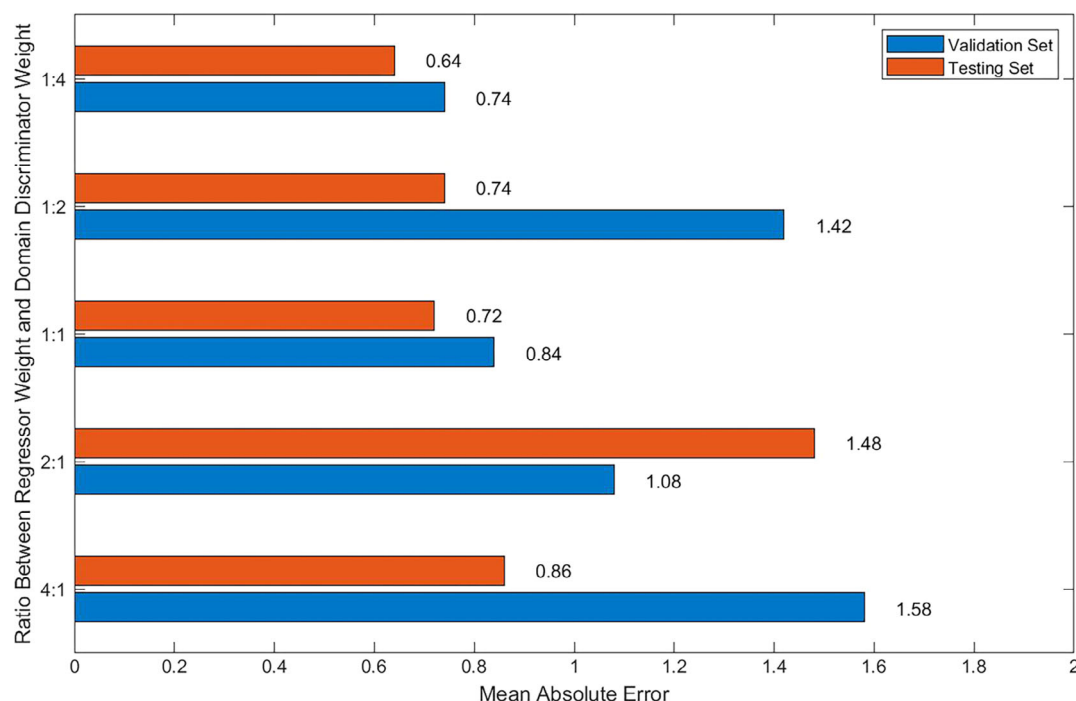


Figure 7. Mean absolute error of the proposed neural network structure with different ratios between the output weight of the regressor and the output weight of the domain discriminator.

the procedure complex and may induce patient discomfort. This study developed a novel ex vivo method to measure the IAP of patients based on the mm-wave FMCW radar. The acquired abdominal displacement signal was processed via the PCG-DANN to predict the corresponding IAP of the patient. Experiments on pigs demonstrated that the proposed method achieves superior performance over other neural network structures and the most adopted sensor-based measuring approaches. The superior performance and inherited convenience of the proposed method render this novel technique an extensive application prospect in future ICUs. However, given the difference between patients in the clinical environment and experimental animals, more research should be conducted to further verify the effectiveness of the proposed method.

Acknowledgements

H.T. and Y.D. contributed equally to this work. This work was supported in part by the Joint Research Fund in Astronomy (U1831117) under a cooperative agreement between the National Natural Science Foundation of China (NSFC), the National Natural Science Foundation of China (Nos. 51877015), the National College Student Innovation and Entrepreneurship Training Program (202110611060) and Clinical Technology Innovation and Cultivation Project of Army Medical University (cx2019js109).

Conflict of Interest

The authors declare no conflict of interest.

Data Availability Statement

Research data are not shared.

Keywords

abdominal wall, data processing, intra-abdominal pressure, machine learning, material informatics, passive mechanical behavior

Received: October 18, 2021

Revised: December 21, 2021

Published online:

- [1] A. W. Kirkpatrick, D. J. Roberts, J. De Waele, R. Jaeschke, M. L. Malbrain, B. De Keulenaer, J. Duchesne, M. Bjorck, A. Leppaniemi, J. C. Ejike, M. Sugrue, M. Cheatham, R. Ivatury, C. G. Ball, A. Reintam Blaser, A. Regli, Z. J. Balogh, S. D'Amours, D. Debergh, M. Kaplan, E. Kimball, C. Olvera, *Intensive Care Med.* **2013**, 39, 1190.
- [2] C. Song, A. Aljani, T. Frank, G. B. Hanna, A. Cuschieri, *Surg. Endosc.* **2006**, 20, 987.
- [3] M. L. N. G. Malbrain, J. J. De Waele, A. W. Kirkpatrick, *Best Pract. Res. Clin. Anaesthesiol.* **2013**, 27, 249.
- [4] J. Pfeifer, L. Oliveira, *Constipation*, Springer, London **2006**.
- [5] J. Wauters, L. Spincemaille, A. S. Dieudonne, K. Van Zwam, A. Wilmer, M. L. Malbrain, *Crit. Care Res. Pract.* **2012**, 2012, 181563.
- [6] J. Novak, J. Jacisko, A. Busch, P. Cerny, M. Stribny, M. Kovari, P. Podskalska, P. Kolar, A. Kobesova, *Clin. Biomech.* **2021**, 88, 105426.
- [7] H. Tang, D. Liu, Y. Guo, H. Zhang, Y. Li, X. Peng, Y. Wang, D. Jiang, L. Zhang, Z. Wang, *Med Devices (Auckl)* **2021**, 14, 119.

- [8] H. Kaneko, *Respir Care* **2014**, 59, 1133.
- [9] U. Klinge, M. Müller, C. Brücker, V. Schumpelick, *Hernia* **1998**, 2, 11.
- [10] G. Wang, J. Muñoz-Ferreras, C. Gu, C. Li, R. Gómez-García, *IEEE Trans Microw Theory Tech* **2014**, 62, 1387.
- [11] E. Turppa, J. M. Kortelainen, O. Antropov, T. Kiuru, *Sensors* **2020**, 20, 6505.
- [12] S. Hazra, A. Santra, in *Proc. of the 18th IEEE Int. Conf. on Machine Learning and Applications (ICMLA)*, IEEE, Piscataway, NJ **2019**.
- [13] Y. H. Kwak, W. Kim, K. B. Park, K. Kim, S. Seo, *Biosens. Bioelectron.* **2017**, 94, 250.
- [14] S. Yamashita, US 8620401, **2013**.
- [15] Y. Wang, W. Wang, M. Zhou, R. Aihu, T. Zengshan, *Sensors* **2020**, 20, 2999.
- [16] A. Ahmad, J. C. Roh, D. Wang, A. Dubey, in *Proc. of the 2018 IEEE Radar Conf. (RadarConf18)*, IEEE, Piscataway, NJ **2018**.
- [17] J. Li, S. Qiu, C. Du, Y. Wang, H. He, *IEEE Trans. Cogn. Develop. Syst.* **2019**, 12, 344.
- [18] X. Chai, Q. Wang, Y. Zhao, X. Liu, O. Bai, Y. Li, *Comput. Biol. Med.* **2016**, 79, 205.
- [19] X. Chai, Q. Wang, Y. Zhao, Y. Li, D. Liu, X. Liu, O. Bai, *Sensors* **2017**, 17, 1014.
- [20] S. Todros, N. de Cesare, G. Concheri, A. N. Natali, P. G. Pavan, *J. Mech. Behav. Biomed. Mater.* **2020**, 103, 103578.
- [21] S. G. Mallat, *A Theory for Multiresolution Signal Decomposition: The Wavelet Representation*, Princeton University Press, Princeton, NJ **2009**.
- [22] J. J. Q. Yu, Y. Hou, A. Y. S. Lam, V. O. K. Li, *IEEE Trans. Smart Grid* **2017**, 10, 1694.
- [23] J. Blitzer, R. McDonald, F. Pereira, in *Proc. of the 2006 Conf. on Empirical Methods in Natural Language Processing*, ACL, Sydney **2006**.
- [24] L. Bruzzone, M. Marconcini, *IEEE Trans. Pattern Anal. Mach. Intell.* **2009**, 32, 770.
- [25] X. Glorot, A. Bordes, Y. Bengio, in *Proc. of the 28th Int. Conf. on Machine Learning (ICML)*, ICML, Bellevue **2011**.
- [26] B. Gong, Y. Shi, F. Sha, K. Grauman, in *Proc. of the 2012 IEEE Conf. on Computer Vision and Pattern Recognition*, IEEE, Piscataway, NJ **2012**.
- [27] Y. Ganin, E. Ustinova, H. Ajakan, P. Germain, H. Larochelle, F. Laviolette, M. Marchand, V. Lempitsky, *J. Mach. Learn. Res.* **2016**, 17, 2096.
- [28] B.-D. Shai, B. John, C. Koby, P. Fernando, *Adv. Neural Inf. Process Syst.* **2007**, 9, 137.
- [29] M. Liang, Hu X., in *Proc. of the IEEE Conf. on Computer Vision and Pattern Recognition*, IEEE, Bostin **2015**.
- [30] M. Sundermeyer, R. Schlüter, H. Ney, in *Proc. of the 13th Annual Conf. of the Int. Speech Communication Association*, ISCA, Portland **2012**.
- [31] K. Choi, G. Fazekas, M. Sandler, K. Cho, (Preprint) arXiv:1703.09179, **2017**.
- [32] Q. Li, L. Shen, S. Guo, Z. Lai, in *Proc. of the IEEE/CVF Conf. on Computer Vision and Pattern Recognition*, IEEE, Seattle, **2020**.
- [33] D. D. N. De Silva, S. Fernando, IT. S. Piyatilake, A. V. S. Karunaratne, in *Proc. of the Eleventh Int. Conf. on Machine Vision (ICMV 2018)*, SPIE, Munich **2019**.
- [34] J. S. Camacho-Juárez, B. Alexander-Reyes, A. Morante-Lezama, M. Méndez-García, H. González-Aguilar, I. Rodríguez-Leyva, O. F. Nuñez-Olvera, C. Polanco-González, L. A. Gorordo-Delsol, J. A. Castañón-González, *Cirugia y Cirujanos* **2020**, 88, 7.
- [35] C. R. Deeken, S. P. Lake, *J. Mech. Behav. Biomed. Mater.* **2017**, 74, 411.
- [36] J. Hu, L. Shen, G. Sun, in *Proc. of the IEEE Conf. on Computer Vision and Pattern Recognition*, IEEE, Piscataway, NJ **2018**.